Welding Behavior and Microstructure of a Ni_3Al Alloy

The addition of hafnium improves the HAZ crack resistance of Ni_3Al alloy

BY M. L. SANTELLA, J. A. HORTON AND S. A. DAVID

ABSTRACT. Recent successes in producing ductile polycrystalline Ni_3Al alloys have led to growing interest in using these materials for structural components. Studying the welding behavior of Ni_3Al alloys is an integral part of developing them as engineering materials. This paper describes the welding behavior and microstructure of a Ni_3Al alloy (known as IC-50) containing 0.1 at.-% boron and 0.5 at.-% hafnium. Gas tungsten arc and electron beam welds were made on annealed sheet, bar material made by consolidating IC-50 powder by hot extrusion, and specimens from a casting. Crack-free welds were made on the sheet and bar, and comparison with previous work indicated that the hafnium addition imparted cracking resistance to these alloys. Crack-free welds were not obtained in the casting, and this behavior was attributed to microsegregation in the base material. Examination of fusion zone microstructures indicated that a distinct microsegregation pattern developed in the welds and affected their ordering behavior. Room-temperature tensile testing indicated that the weld fusion zones are ductile and that weld test specimens can have strength and ductility comparable to those of base materials.

Introduction

There has been interest in the development of Ni_3Al for engineering applications since the discovery that its yield strength increases with temperature up to about 600°C (1112°F) (Ref. 1). Besides unusual strength behavior, good creep and oxidation resistance have also been identified with this intermetallic compound (Ref. 2). Typically, Ni_3Al single crystals exhibit very good room-temperature ductility (Ref. 2). However, other studies of mechanical behavior (Refs. 3, 4) established that polycrystalline Ni_3Al generally failed by brittle intergranular fracture with little or no ductility. The reason for the brittle behavior is that grain boundaries in polycrystalline Ni_3Al are intrinsically weak (Refs. 5, 6), and this characteristic has been the major impediment to the development of Ni_3Al alloys for structural uses.

Recent studies (Refs. 5, 7) have shown that boron, added as a few hundred parts per million to polycrystalline Ni_3Al, can dramatically improve the resistance of the alloy to brittle intergranular fracture by segregating to grain boundaries and improving their strength relative to the matrix. This discovery has stimulated interest in the development of Ni_3Al alloys (Refs. 2, 5, 8) because of the apparent advantages of this material over conventional alloys, especially for high-temperature applications including steam and gas turbine components, Stirling and low-heat rejection diesel engine components, and a variety of structural components in energy conversion systems. Some of the issues addressed in this alloy development program are hot workability, mechanical properties, oxidation and corrosion behavior, and weldability.

Our work was aimed at assessing weldability, and this paper describes the welding behavior and microstructures of a Ni_3Al alloy considered to have some commercial value (Refs. 2, 8). Previous work (Refs. 8–10) indicated that weld cracking in the heat-affected zone (HAZ) was a major problem for Ni_3Al alloys. For the purposes of this study, the degree of weldability was defined in terms of resistance to cracking. We will show that the resistance of Ni_3Al to HAZ cracking can be improved by alloying with 0.5 at.-% hafnium, that defect-free welds can be made in wrought Ni_3Al alloys by electron beam (EB) and gas tungsten arc (GTA) welding, and that these welds have reasonably good tensile properties at room temperature.

KEY WORDS

Aluminides
Ni_3Al Alloy
IC-50 Alloy
Hafnium Addition
GTA Welds in Ni_3Al
EB Welds in Ni_3Al
Cracking Resistance
Weld HAZ Cracking
Wrought Materials
Weld Microanalysis

Materials and Experimental Details

The alloy used for this study (ORNL designation IC-50) was obtained in three different product forms. One was recrystallized sheet either 0.7 or 2.0 mm (0.03 or 0.08 in.) thick, produced from an arc-melted ingot by repeated cold rolling, with intermediate annealing at 1050°C (1922°F). The second was a bar produced by hot extrusion of a canned powder at 1100°C (2012°F). The high-purity powder was produced by an atomization process. The finished diameter of the bar was 38 mm (1.5 in.), from which 5-mm-thick (0.2-in.) rectangular welding coupons were cut longitudinally. The last form used was a plate casting 12.5 mm (0.5 in.) thick. Welding coupons with thicknesses of 5 and 0.7 mm were cut from the casting. The compositions of the sheet and bar, as determined by standard chemical analysis, are given in Table 1. A nominal composition is given

Table 1—Alloy Compositions (at.-%)

Alloy Form	Composition			
	Ni	Al	Hf	B
Sheet	76.81	22.6	0.52	0.07
Bar	76.60	22.8	0.51	0.09
Casting	77.49	21.9	0.51	0.10

M. L. SANTELLA, J. A. HORTON and S. A. DAVID are with the Metals and Ceramics Division, Oak Ridge National Laboratory, Oak Ridge, Tenn.

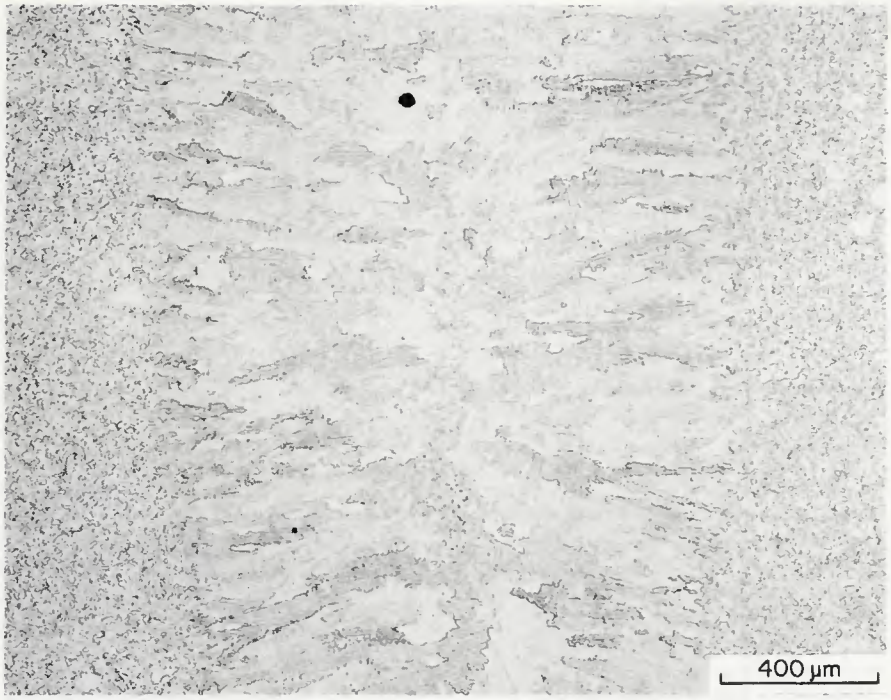

Fig. 1—Microstructure of EB weld in hot-extruded powder coupon of IC-50. Appearance is typical of welds made in this alloy

in Table 1 for the casting. The sheet and bar were single-phase γ', which has the ordered $L1_2$ crystal structure, while the casting contained a small amount of the γ phase in a γ' matrix. The γ phase is the disordered face-centered cubic equivalent of the ordered γ' phase. The grain size of the sheet and casting was ASTM 8 (20 μm). The grain size of the bar was ASTM 9–10 (10–15 μm). The fine grain size of the casting was the result of producing it as a chill casting.

Most of the welds made for this study were autogenous, *i.e.,* made without a filler metal. However, some GTA welds were made on the 2-mm sheet using a filler metal made by shearing strips from the rolled sheet. The size of this filler was approximately 2 mm square. All GTA welds were made with argon shielding and standard welding practices. The EB welds were made in a Leybold-Heraeus 15-kW welding machine.

Specimens for optical metallography were etched by swabbing with glyceregia (10 mL HNO_3, 20 mL HCl and 30 mL glycerol) to show general microstructure, or were etched electrolytically with an oxalic acid solution (10 g oxalic acid and 100 mL H_2O) to show solidification microstructures. Specimens for transmission electron microscopy (TEM) were thinned to perforation with a perchloric acid solution (Ref. 5). A scanning electron microscope (SEM) was used to examine metallographically prepared samples and fracture surfaces and to perform energy-dispersive spectroscopy (EDS) using standard routines. Some wavelength-dispersive spectroscopy (WDS) was also done with an electron probe microanalyzer (EPMA).

Postweld heat treatments were done in a vacuum muffle furnace. Tensile tests were conducted at room temperature on an Instron testing machine with a crosshead speed of 42 μm/s.

Results

Welding

Initially, the welding behavior of IC-50 was assessed by making a series of full penetration autogenous welds on the 0.7-mm wrought sheet. EB welds were made at speeds of 2.1, 4.2, 10.6, 21.2 and 42.5 mm/s (0.08, 0.2, 0.4, 0.8 and 1.7 in./s), and automatic GTA welds were made at 4.2 mm/s. Examination of the as-welded surfaces at 100X showed the welds to be free of cracks, except for a few crater cracks at the termination points of the EB welds made at 21.2 and 42.5 mm/s. Only full penetration EB welds were made in the consolidated powder product, and they were free of defects except for some isolated porosity. Several manual GTA welds were made in the 2-mm sheet with the IC-50 filler previously described. Optical as well as radiographic examination showed that these GTA welds were also crack-free. The behavior of the wrought forms of IC-50 suggested that this alloy has reasonably good weldability.

Only autogenous GTA welds were made on the cast material: partial penetration welds were made on the 5-mm-thick coupons, and full penetration welds were made on the 0.7-mm-thick coupons. All of these welds had a high incidence of cracking. Although the cast material had a tendency to crack upon welding, it was possible to cold roll it to a reduction of about 10% without cracking at room temperature. The response to cold rolling indicated that there was enough boron at grain boundaries to prevent the casting from being completely brittle.

Table 2—Results of Microanalysis in Weld Fusion Zone and Matrix (at.-%)

Location	Composition		
	Ni	Al	Hf
Dendrite core	79.69	20.15	0.16
Intermediate	77.28	22.49	0.23
Interdendritic	77.65	20.75	1.60
Matrix	77.65	21.80	0.55
Chemical analysis[a]	76.81	22.60	0.52

(a) Results of matrix chemical analysis by standard techniques.

Microstructure of Wrought Materials

Optically, the fusion zone microstructures of welds in IC-50 were similar in appearance, regardless of the type of material on which they were made, or whether they were made by GTA or EB welding, or with or without filler metal. A cross-sectional view of the microstructure of an EB weld made in the hot-extruded powder bar is shown in Fig. 1. Large columnar grains are seen extending into the fusion zone from the base material, and the dendritic solidification substructure of the fusion zone is visible. Examination of the HAZ indicated that there was no detectable grain growth or precipitation of second phases in this region of the microstructure.

Figure 2 (left) shows a more detailed view of solidification substructure from a GTA weld fusion zone. The dendritic nature of the microstructure is clearly evident, as the dendrite cores appear darker than the interdendritic regions. Figure 2 (right) shows the appearance of this region, at higher magnification, when imaged with backscattered electrons in a SEM. Microprobe analysis was used to show that the light interdendritic regions of Fig. 2 (right) were highly enriched with hafnium, while the dendrite cores were enriched with nickel. The dark band surrounding the dendrite cores corresponded to a zone high in aluminum content. The microprobe data for the fusion zone and the matrix are given in Table 2, where the data for each location represent an average value of many analyses. The location termed intermediate corresponds to the dark band encircling the dendrite cores, which is enriched in aluminum by about 2.0 at.-% relative to other regions of the fusion zone microstructure.

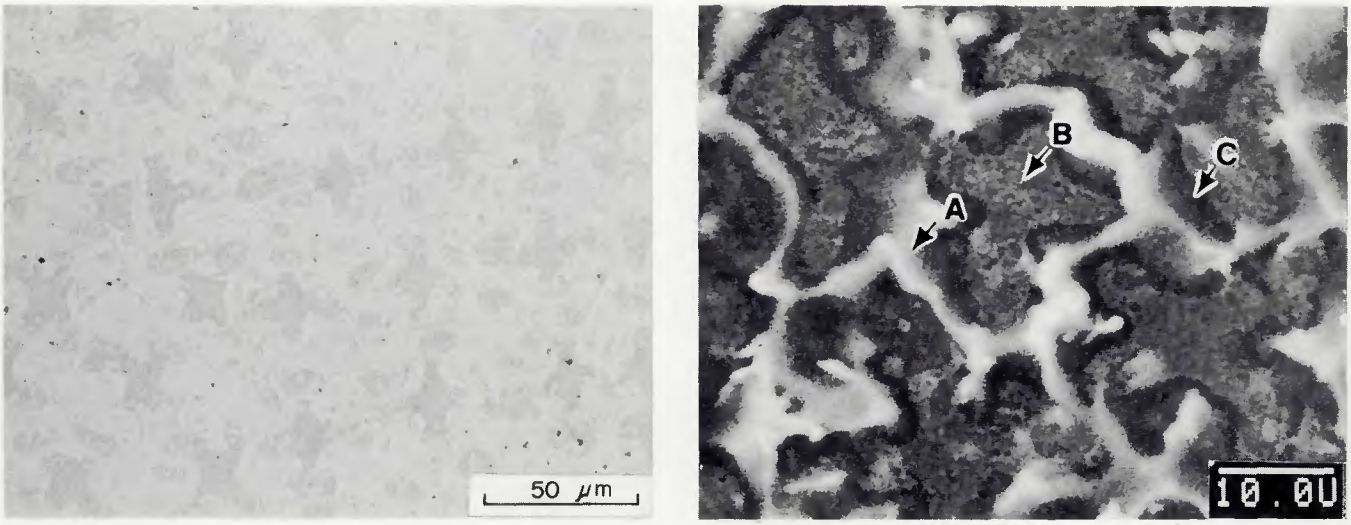

Fig. 2 — Solidification structure in fusion zone of GTA weld made with addition of filler metal. Left — Optical micrograph; right — backscattered electron image, where (A) represents interdendritic regions, (B) represents dendrite core regions, and (C) represents intermediate regions. Appearance is typical of welds made in this alloy

The microstructures of EB and GTA welds in the wrought materials were also similar in appearance when they were imaged in TEM. The micrograph shown in Fig. 3, taken in an EB weld in the hot-extruded powder material, typifies the appearance of the fusion zone microstructures. Our initial analysis (Ref. 11) indicated that the entire fusion zone microstructure was ordered in the as-welded condition, but while the dendrite core regions (A in Fig. 3) contained a large number of relatively small domains, the interdendritic regions (B) were devoid of antiphase boundaries. Dislocations were visible throughout the microstructure.

Subsequent annealing of the welds for 1 h at 950°C (1742°F), however, yielded two-phase microstructures. The microstructure of a dendrite core region in an EB weld after annealing at 950°C for 1 h is shown in the bright-field/dark-field pair of micrographs in Figs. 4A and B. The bright-field micrograph, Fig. 4A, indicates that a network similar to an antiphase boundary structure was present in the microstructure after annealing. The dark-field image (Fig. 4B), taken with a {100} (cube plane type of) superlattice reflection, confirms that the dark features are actually a network of disordered material rather than domain boundaries. The disordered material formed a three-dimensional network and was atomically coherent with the ordered matrix. The structure of the disordered zones was that of the face-centered-cubic nickel solid-solution γ phase, which is the disordered equivalent of the ordered matrix.

Dendrite core regions in an autogenous GTA weld in annealed sheet material before and after annealing at 950°C for 1 h are shown in Figs. 5A and B. A network of disordered γ phase is visible in both, but the random arrangement found in the as-welded condition (Fig. 5A) was changed after annealing to a microstructure where the disordered regions are slightly coarsened and aligned on {100} planes in the face-centered-cubic lattice — Fig. 5B.

Microstructure of the Plate Casting

The microstructure of an autogenous GTA weld made in the thin-plate cast material is shown in Fig. 6. A large intergranular crack is visible extending from the fusion zone into the HAZ. Many smaller intergranular cracks, 10 to 30 μm in length, were also observed in the HAZ. The SEM micrograph in Fig. 7 confirms the intergranular nature of the HAZ cracks, and shows, as might be expected, that the casting was a two-phase material composed of an ordered matrix containing disordered grains. The location of cracks, however, did not appear related to the presence of the second-phase grains.

The microstructure of the cast material is shown in the backscattered electron image given in Fig. 8. The dendritic nature of the cast microstructure is evident, and as in the weld fusion zones previously described, the light areas correspond to regions of hafnium segregation. A web-like structure appeared to be associated

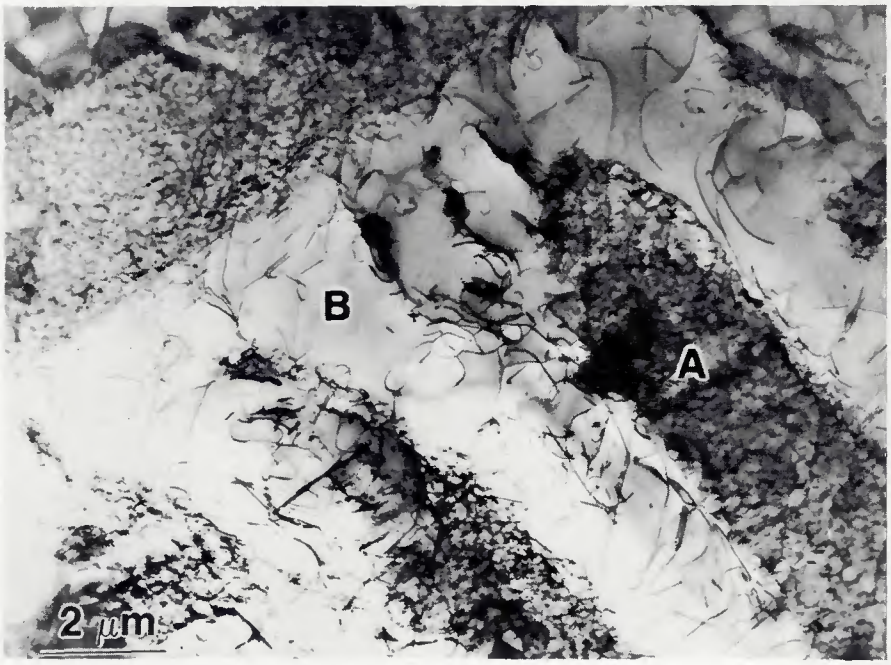

Fig. 3 — TEM micrograph in fusion zone of EB weld made in hot-extruded powder material, where (A) represents dendrite core regions and (B) represents interdendritic regions. Appearance is typical of EB or GTA welds made in IC-50

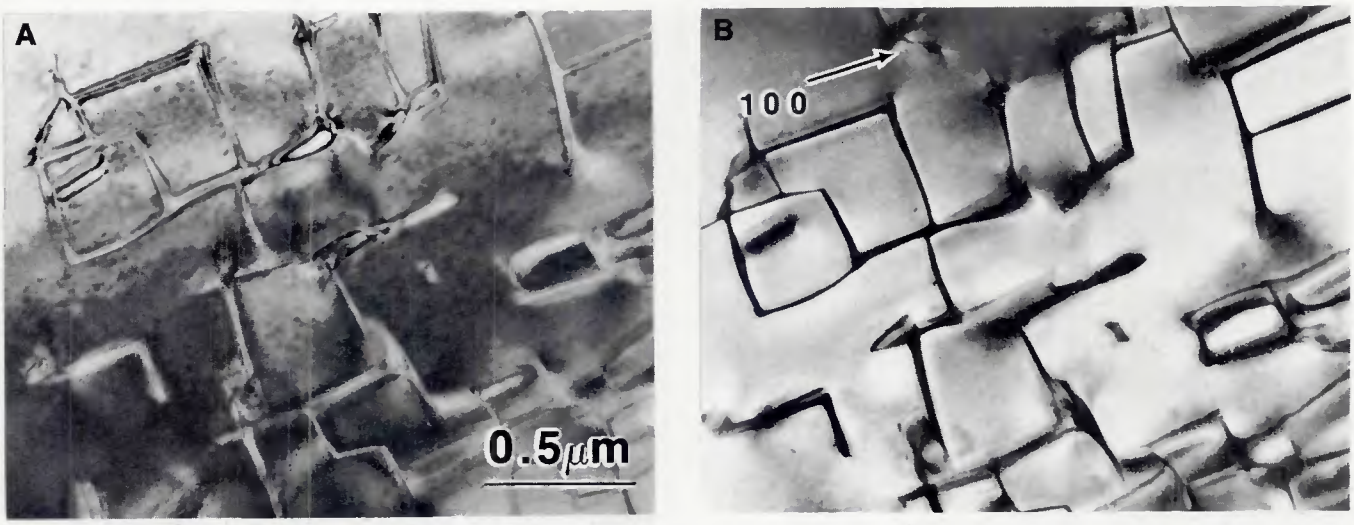

Fig. 4 — Microstructure of dendrite core in EB weld after annealing at 950°C for 1 h. A — Bright-field TEM micrograph; B — dark-field TEM micrograph using {100} superlattice reflection of same area as A. Dark areas are disordered while bright areas are ordered. Electron beam direction is near [001]

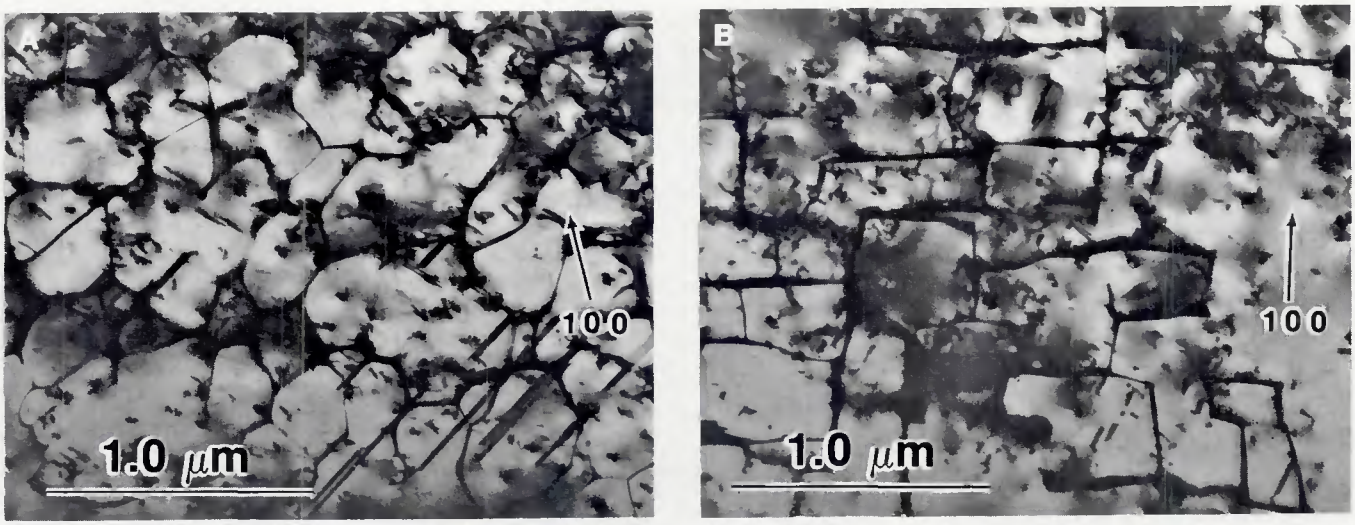

Fig. 5 — Dark-field TEM micrographs using {110} superlattice reflection of dendrite cores in GTA weld before (A), and after (B) annealing at 950°C for 1 h. Electron beam direction is near [001] in both micrographs

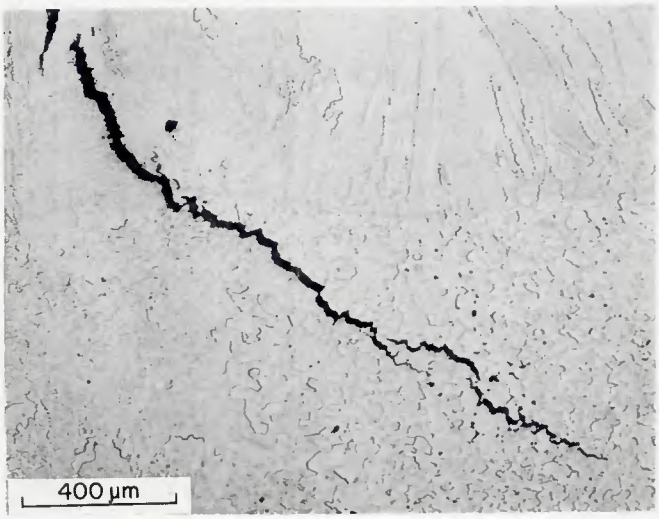

Fig. 6 — Microstructure of GTA weld in the thin-plate casting showing large intergranular crack in heat-affected zone extending into the fusion zone

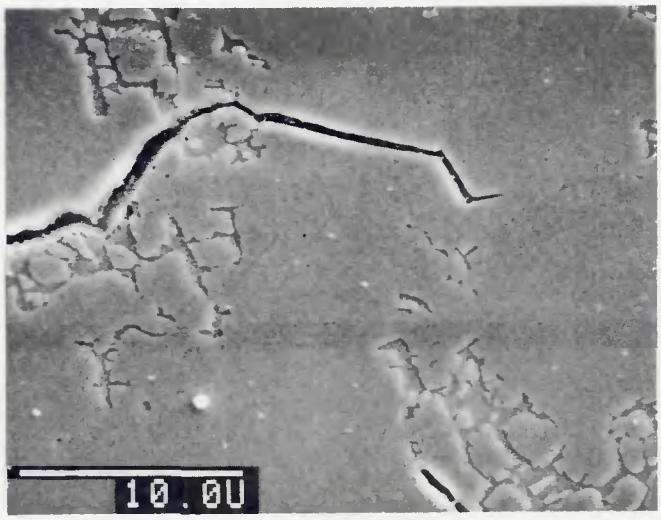

Fig. 7 — SEM micrograph on polished surface showing heat-affected zone crack tip in thin-plate casting and presence of second phase

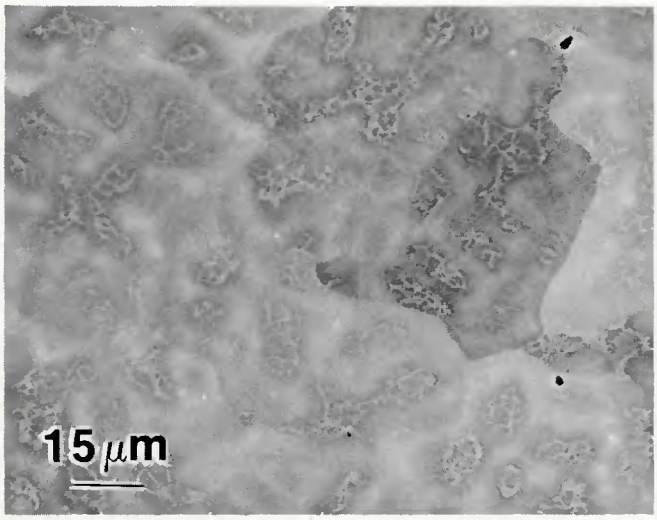

Fig. 8—Backscattered electron image of thin-plate casting showing pattern of microsegregation. Light areas are enriched in hafnium. Dendrite core regions are enriched in nickel and are two-phased

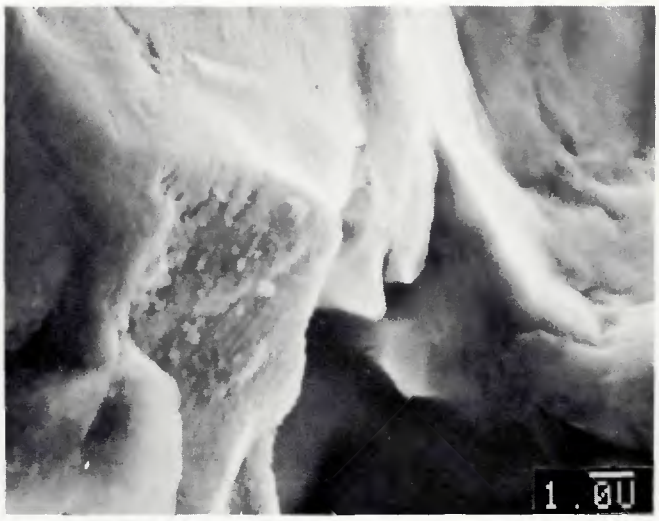

Fig. 9—SEM micrograph of grain surfaces from a crack in the heat-affected zone of the thin-plate casting

with the dendrite cores, and it presumably is the disordered phase. Figure 8 indicates that the microstructure of the casting is inhomogeneous, and that while hafnium segregation to grain boundaries is apparent in some areas, its occurrence at these sites is not a general feature. The grain boundaries of the casting are more or less randomly distributed throughout the solidification substructure.

HAZ cracks like those shown in Figs. 6 and 7 were broken open, by notching specimens near crack tips and fracturing by impact, so that their internal surfaces were exposed and could be examined in the SEM. Figure 9 shows the appearance of a HAZ crack surface. The intergranular nature of the crack is apparent, and there is no indication that failure was associated with liquation due to either segregation or dissolution of second-phase particles along the grain boundaries.

Tensile Tests

The results of room-temperature tensile tests of IC-50 weldments made in wrought material are given in Table 3, along with typical tensile properties of recrystallized IC-50 sheet. The orientation of the test specimens was such that the weld axis was either perpendicular (transverse) or parallel (longitudinal) to the tensile axis, as indicated in Table 3. The EB weld specimen had gauge dimensions of 19.0 × 6.4 × 4.4 mm (0.75 × 0.25 × 0.17 in.). The transverse GTA weld specimens had gauge dimensions of 19.0 × 4.8 × 1.3 mm (0.75 × 0.19 × 0.05 in.). The EB weld specimen and the transverse GTA weld specimens all fractured across the fusion zone. The fracture appearance of the EB weld specimen is shown in Fig. 10, and its dimpled appearance indicates that the fusion zone failed by ductile void coalescence. The longitudinal GTA weld specimens had gauge dimensions of 12.7 × 3.6 × 0.7 mm (0.5 × 0.14 × 0.03 in.). The bead width of these welds was slightly less than the tensile specimen gauge width so that the entire weldment was tested. One specimen was given a postweld heat treatment of 1 h at 950°C (1742°F) before testing. All of the longitudinal GTA weld specimens broke in the gauge section.

Discussion

A plot of weld cracking frequency (Fig. 11) taken from the work of David and co-workers (Ref. 9) shows that crack-free welds were not obtained in Ni_3Al alloys containing only boron as an intentional addition. Comparison with our data from IC-50 indicates that the hafnium addition

Table 3—Results of Tensile Testing IC-50 Weldments

Specimen	Condition	Proportional Limit (MPa)	Tensile Strength (MPa)	Elongation (%)
EB, T	AW	140	1057	24
GTA, T	AW	142	1294	28
GTA, L	AW	318	1292	34
GTA, L	PWHT	311	1413	43
Base		200–350	1380	40–50

EB = electron beam weld.
GTA = gas tungsten arc weld.
T = tensile axis perpendicular to weld axis.
L = tensile axis parallel to weld axis.
AW = as-welded.
PWHT = postweld heat treated.

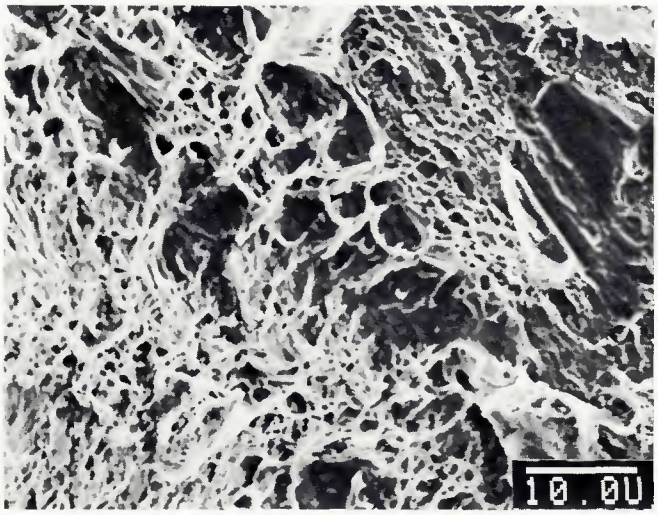

Fig. 10—SEM micrograph of fractured weld showing evidence of ductile void coalescence in fusion zone

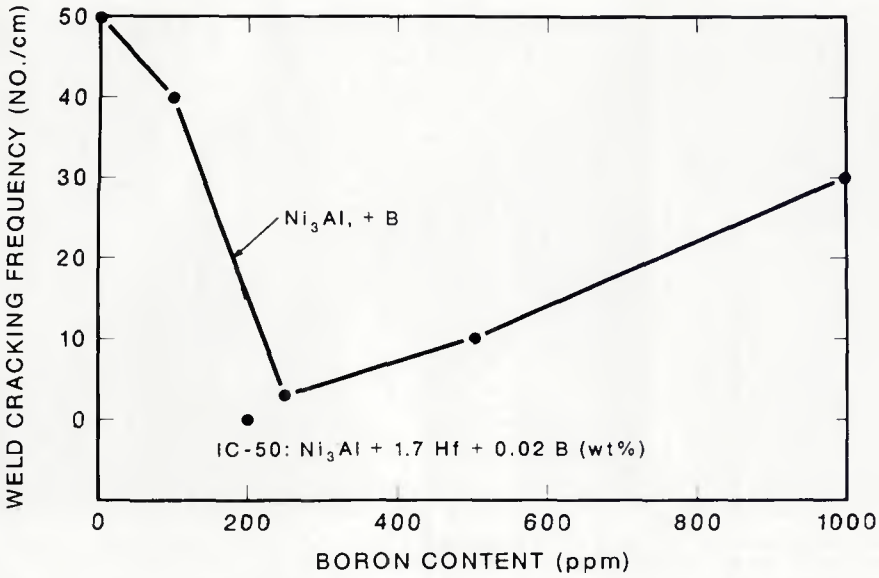

Fig. 11—Cracking frequency plotted against boron concentration for Ni_3Al + B alloy welds (taken from Ref. 9). Behavior of wrought IC-50 is also indicated

of 0.5 at.-% clearly improved the weldability, *i.e.*, resistance to HAZ cracking, of the wrought Ni_3Al + B alloys. Hafnium was added to the base alloy because it improves high-temperature strength by solid solution hardening (Ref. 2). Good high-temperature strength is an important factor in increasing the resistance of alloys to HAZ cracking (Ref. 10), and the hafnium addition appears to be an effective way of achieving this in Ni_3Al alloys.

Our study of welding behavior showed that autogenous EB and GTA welds could be made in IC-50 sheet with relative ease. The study suggested that the same may be said for welding of the hot-extruded powder product, although our experience with this type of material was more limited. It also showed that the use of IC-50 filler metal for GTA welding is possible without taking any unusual precautions from a welding standpoint, and that acceptable welds can be made in wrought IC-50 base material by this approach. On the other hand, the occurrence of crater cracks in some of the high-speed EB welds and the susceptibility of the cast material to cracking indicate that the resistance of IC-50 to cracking is not as high as that of many commercial superalloys. Overall, these observations provide encouragement for the development of weldable Ni_3Al alloys.

The variation of microstructure in the weld fusion zones can be explained by considering the microsegregation pattern that developed during weld solidification and by comparing weld microstructures before and after annealing. For Ni_3Al alloys containing less than 25 at.-% aluminum, a nickel-enriched disordered phase is the first solid to form (Refs. 12, 13). Horton and co-workers have shown (Ref. 15) that nickel-enriched regions in rapidly solidified Ni_3Al alloys undergo ordering at lower temperatures than regions depleted in nickel, and that those regions which order at low temperatures contain well-defined antiphase boundary structures because of restricted domain growth. Our microprobe data confirmed that, in IC-50 weld fusion zones, dendrite cores were nickel enriched, while interdendritic regions were enriched with aluminum or hafnium relative to the base composition. The variation of microstructure in the weld fusion zones observed by TEM (Fig. 3) agreed, qualitatively, with the microsegregation observations because the aluminum- and hafnium-enriched interdendritic regions were clearly single-phase γ' containing no antiphase boundaries, while the nickel-rich dendrite cores appeared to contain a large number of small ordered domains.

TEM examination of the GTA weld microstructures after annealing showed that the dendrite core regions were actually two-phased. Because of this observation, specimens of the base alloy, which were given the same heat treatment of 1 h at 950°C, were also examined in the TEM. The base material was single-phased before and after heat treatment, indicating that annealing IC-50 for 1 h at 950°C will not transform the single-phase structure to a two-phase structure. We expect that this behavior would hold for weld fusion zones also and that the two-phase microstructures observed after annealing existed in the as-welded state, *i.e.*, before heat treatment. Our problem in identifying these features as disordered phase in the as-welded microstructure was due to the difficulty of differentiating in TEM between an antiphase boundary and a narrow band of disordered material. Annealing the welds overcame this difficulty. The combination of our microprobe and TEM data from the IC-50 welds showed that the microsegregation that developed during solidification of the welds produced a fine-scale network of disordered γ phase in the ordered matrix in dendrite core regions of the microstructure, while interdendritic regions were fully ordered after solidification.

Comparison of fusion microstructures before and after annealing for 1 h at 950°C also indicated that the interfaces between the network of disordered γ phase and the ordered matrix tended to reorient during annealing from a random orientation to an aligned orientation on {100} planes. The alignment of these interfaces on {100} planes during annealing is similar to the behavior of disordered regions in other nickel-based ordered alloys having the $L1_2$ structure (Refs. 15, 16), and it indicates that this arrangement minimizes the total interfacial energy.

With regard to the thin-plate casting, it was concluded that grain size was not an important factor in the low crack resistance of this material because its grain size was in the same range as that of the wrought sheet and hot-extruded material (ASTM 8–10). The differences between the casting and the wrought materials were that the casting contained a pronounced microsegregation pattern for nickel, aluminum and hafnium, and the microstructure was two-phase. Backscattered electron imaging and microanalysis showed that grain boundaries were randomly associated with the microsegregation pattern of the casting. Examination of HAZ crack surfaces confirmed that liquation was not responsible for the low cracking resistance of the casting and indicated that there was no significant precipitation of second phases on grain boundaries that may have caused their embrittlement. No grain boundary phases were observed on polished sections either.

Some insight into the behavior of the casting may be gained by considering work of Liu and co-workers (Ref. 5) showing that the tensile ductility of Ni_3Al + B alloys was dramatically reduced as the aluminum concentration approached or exceeded 25 at.-%. It is reasonable to expect a similar effect of stoichiometry on the ductility of IC-50. Hafnium is known to preferentially occupy aluminum sublattice sites in Ni_3Al alloys (Ref. 17). It may be, therefore, that grain boundary segments in the IC-50 casting where the local level of aluminum sublattice occupants (*i.e.*, aluminum and hafnium) exceeded 25 at.-% due to microsegregation were relatively brittle, and therefore, had reduced capacity for accom-

modating the stresses induced during welding. Another important factor that could lead to a difference in cracking resistance between the casting and the wrought materials is the distribution of boron. Although the casting and the wrought sheet had the same grain size, ASTM 8, the ductility of the casting (~10%) was much less than that of the wrought material (40–50%). Because the ductility of Ni_3Al alloys also is a strong function of boron concentration (Ref. 5), the low ductility of the casting may be a direct result of its having a grain boundary boron concentration that has not been optimized by the beneficial effects of heat treatment and deformation processing. Although the exact cause of the increased tendency of the casting to crack during welding could not be determined, the lower ductility of the casting compared to wrought sheet material seems to play a critical role.

The tensile properties of the IC-50 weldments compared well with the typical properties of recrystallized sheet. The elongation values of all the weld tensile specimens were very good, indicating that the weld fusion zones were reasonably ductile. This point was confirmed by examination of the fractured specimens in the SEM. Also, the ultimate tensile strength of the welds was within a few percent of the base metal properties, except for the transverse EB weld. In that case, the lower strength may be characteristic of the hot-extruded powder product. The yield strength of the transverse weld specimens was significantly lower than that of the base material. The yield strength of Ni_3Al alloys varies inversely with grain size (Ref. 5), and this may explain the low yield strength of the transverse welds, because the grain size was very large in the fusion zones of all of them. Microsegregation in the fusion zones may also influence weld properties. The longitudinal welds had yield strength values within the range of the base material properties. However, the fusion zones did not occupy the full cross-section of these specimens, making it difficult to form conclusions about these data relative to the base material. In spite of this complication, the longitudinal specimens do indicate that the tensile strength and ductility of IC-50 welds can benefit from postweld heat treatments.

Conclusion

The significant findings of our study of the welding behavior and microstructure of a Ni_3Al alloy containing 0.5 at.-% Hf + 0.1 at.-% B, known as IC-50, are:

1) The addition of 0.5 at.-% Hf to a Ni_3Al + B alloy improved its resistance to HAZ cracking.

2) Crack-free autogenous welds were made in wrought sheet of IC-50 by EB and automatic GTA welding. Crack-free EB welds were also made in coupons of compacted IC-50 powder produced by hot extrusion.

3) Filler metal was fabricated from wrought IC-50 sheet and used to make manual GTA welds in IC-50 base metal that were free of defects.

4) Microanalysis showed that in the weld fusion zone microstructures, aluminum and hafnium segregated to interdendritic regions, while nickel enrichment was found at dendrite cores.

5) In weld fusion zones, microsegregation resulted in two-phase microstructures with nickel-rich dendrite cores containing a network of disordered γ phase that was coherent with the ordered γ' matrix. Interdendritic regions were fully ordered after solidification. A postweld heat treatment of 1 h at 950°C would not eliminate the γ-phase network, but caused alignment of its interfaces on {100} planes in the ordered matrix.

6) The high cracking susceptibility of cast material was attributed to embrittlement of the grain boundaries, resulting from microsegregation.

7) Room-temperature tensile testing showed that the strength and ductility of IC-50 welds compare favorably with base material properties. Postweld heat treatment for 1 h at 950°C improved the tensile properties of IC-50 weld specimens.

Acknowledgments

The authors wish to thank C. T. Liu for his technical support, J. M. Vitek for discussions about the microanalysis data, T. J. Henson and B. C. Leslie for assistance with the microprobe and SEM, J. A. Carpenter, R. W. Swindeman and J. H. Schneibel for their technical reviews, and Kathy Gardner for preparing the final manuscript. This work was sponsored jointly by the U.S. Department of Energy AR&TD Fossil Energy Program and the Energy Conversion and Utilization Technologies (ECUT) Program under contract DE-AC05-84OR21400 with Martin Marietta Energy Systems, Inc.

References

1. Flinn, P. A. 1960. *Trans. AIME,* 218, 145.
2. Liu, C. T., and Stiegler, J. O. 1984. *Science,* 226, 636.
3. Westbrook, J. H. 1957. *Trans. AIME,* 209, 898.
4. Grala, E. M. 1960. *Mechanical Properties of Intermetallic Compounds.* J. H. Westbrook, ed. John Wiley and Sons, Inc., New York, N.Y., p. 358.
5. Liu, C. T., White, C. L., and Horton, J. A. 1985. *Acta Metall.,* 33, 213.
6. Ogura, T., Hanada, S., Masumoto, T., and Izumi, O. 1985. *Met. Trans. A,* 16A, 441.
7. Aoki, K., and Izumi, D. 1979. *Nippon Kinzaku Gakkaishi,* 43, 1190.
8. Liu, C. T., Jemian, W. A., Inouye, H., Cathcart, J. V., David, S. A., Horton, J. A., and Santella, M. L. 1984. Initial development of nickel and nickel-iron aluminides for structural uses. ORNL-6067.
9. David, S. A., Jemian, W. A., Liu, C. T., and Horton, J. A. 1985. *Welding Journal* 64(1):22-s to 28-s.
10. Santella, M. L., and David, S. A. 1986. A study of heat-affected zone cracking in Fe-containing NiAl alloys. *Welding Journal* 65(5):129-s to 137-s.
11. Santella, M. L., and David, S. A. 1986. Advances in welding science and technology. *Proceedings of an International Conference on Welding Research,* p. 629, Gatlinburg, Tenn. May 18–22, 1986, S. A. David, ed. ASM International, Metals Park, Ohio.
12. Hansen, M. 1958. *Constitution of Binary Alloys.* McGraw-Hill Book Co., New York, N.Y.
13. *ASM Metals Handbook,* Vol. 8, 1973. Metallography, structures and phase diagrams. ASM International, Metals Park, Ohio.
14. Horton, J. A., and Liu, C. T. 1985. *Acta Metall.,* 33, 2191.
15. Horton, J. A., DasGupta, A., and Liu, C. T. 1984. *Proceedings of the 42nd Annual Meeting of the Electron Microscopy Society of America.* G. W. Bailey, ed., San Francisco Press, San Francisco, Calif., p. 486.
16. Horton, J. A., DasGupta, A., and Liu, C. T. 1985. *High Temperature Ordered Intermetallic Alloys.* C. C. Koch, C. T. Liu, and N. S. Stoloff, eds., Materials Research Society, Pittsburgh, Pa., p. 109.
17. Ochiai, S., Oya, Y., and Suzuki, T. *Acta Metall.,* 32, 289.